Computational structure-activity relationship (SAR) of berberine analogs in double stranded and G-quadruplex DNA binding reveals both position- and target-dependence

Stephanie Sun[1], Bhavesh Ashok[2], Andrew Su[3], Saira Hamid[4], Karthikha Sri Indran[4], Aashi Shah[5], Sarah Su[5], Simrun Sakhrani[6], *Edward* Njoo[7]

[1] BASIS Independent Silicon Valley, San Jose, CA; [2] Amador Valley High School, Pleasanton, CA; [3] Foothill High School, Pleasanton, CA; [4] Mission San Jose High School, Fremont, CA; [5] Los Altos High School, Los Altos, CA; [6] The College Preparatory School, Oakland, CA; [7] Department of Chemistry, Biochemistry, & Physical Science, Aspiring Scholars Directed Research Program, Fremont, CA

ABSTRACT: Berberine, a natural product alkaloid, and its analogs have been reported to have a wide range of medicinal properties, including antibacterial and anticancer effects. It has been previously reported that berberine and its analogs intercalate into DNA, thereby inhibiting DNA replication. Berberine has also been studied as a photosensitizer, generating reactive singlet oxygen in situ, and this has applications in photodynamic therapy. Various groups have synthesized berberine analogs that have comparable or improved biological activity; however, an exhaustive structure-activity relationship (SAR) of DNA binding affinities on berberine analogs with substitution at C-8, C-12, and C-13 has not been previously reported. High throughput virtual screening (HTVS) allows for efficient analysis of compound libraries to identify lead compounds as possible pharmaceutical agents. Here, we employed HTVS towards a library of alkyl or aryl berberine analogs on carbons 8, 12, and 13 to probe binding to double stranded and G-quadruplex DNA. Predicted binding affinities to double stranded DNA and G-quadruplex DNA were generated via molecular docking, excited state electronic structure calculations were conducted via time-dependent density functional theory (TD-DFT) to probe each compound's potential activity as a photosensitizer, and potential G-quadruplex stabilizing abilities of key berberine analogs were probed by molecular dynamics (MD) simulations on a 4.0 ns timescale.

INTRODUCTION

Berberine (1) (Figure 1a and 1b), a naturally occurring isoquinoline alkaloid extracted from the roots and stem of plants from the genus Berberis (Figure 1c), has been of great medicinal interest due to its wide range of reported biological activities, including antimicrobial, antidiabetic and anticancer activity (1,2,3,4,5). Berberine-containing extracts have been used as a medicinal agent in many traditional cultures dating back to 3000 BC (6).
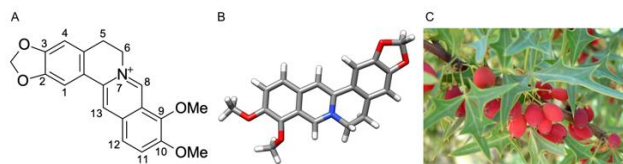

Figure 1. Background and introduction of berberine **1** (a) chemical structure of berberine with the carbons numbered (b) 3D structure of berberine (DFT optimized, B3LYP, def2-SVP) (c) *Berberis trifoliolata*, one example of a plant from which berberine-containing extracts can be obtained (7)

Moreover, berberine was previously found to intercalate in DNA with a high binding affinity, driven by electrostatic attractions and pi-stack interactions between the compound and nucleotide base pairs in DNA secondary structures (8). Upon photoirradiation of the berberine-DNA complex, berberine acts as a photosensitizer and generates singlet oxygen, a reactive oxygen species, which oxidizes guanines and results in DNA damage, thereby inhibiting DNA replication and halting cell division (9). This has been previously studied in application to photodynamic therapy as a potential treatment of various types of cancers and antimicrobial agents (10,11). Berberine has also been reported to stabilize G-quadruplex DNA (G4DNA), which inhibits telomerase, an enzyme that is overexpressed in cancers; this inhibition of telomerase results in the inhibition of cancer activity (12).

Several semisynthetic analogs and derivatives of berberine have previously been prepared and evaluated for biological activities; some of these are reported to have comparable or superior antibacterial, antifungal, or anticancer activity compared to the natural product, and

some have been reported to possess improved binding affinities to DNA and G4DNA. Addition of an alkyl or aryl chain to carbon 8 of berberine can be achieved via nucleophilic addition of alkyl or aryl Grignard; such compounds have been reported to have more potent antimicrobial activity (13), but it is not known what role the stereogenic center at carbon 8 might play in DNA binding (Figure 2a). A library of 12-amine-berberine derivatives studied by Wang et al. have been demonstrated to have more potent anticancer activity (14). The synthesis and biological screening of 13-alkylberberine analogs revealed that the addition of alkyl chains of various lengths improves the anticancer, anti inflammatory, and antioxidant activity of berberine (15,16). It has also been reported that a borohydride reduction at the carbon 8 iminium to yield dihydroberberine (2) generally results in a loss of antimicrobial efficacy (17). While many have studied the biological activities of berberine and its analogs, less than 20 percent of studies reported in the last ten years quantify the DNA-binding affinities of such analogs, and even fewer have produced crystal structures of berberine bound to a DNA target.
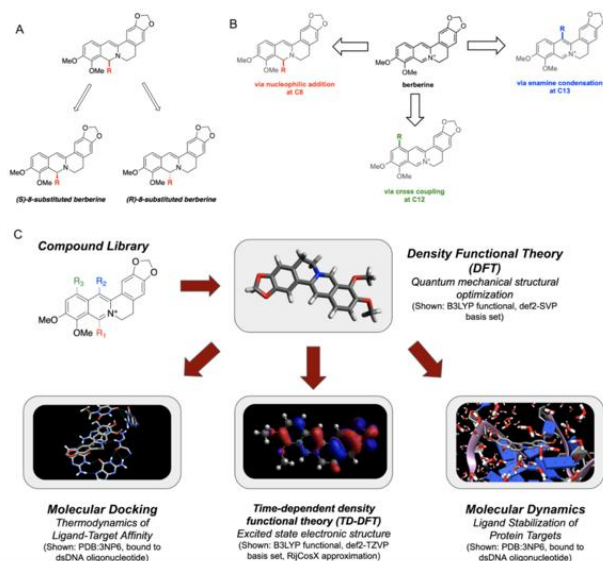
Figure 2. Design of the library of berberine analogs and our methodology in this study. (a) A stereocenter is formed when alkyl and aryl chains are added to carbon 8 of berberine, resulting in R and S enantiomers. Both R and S enantiomers of all carbon 8 analogs were studied. (b) Possible reactions for the synthesis of carbon 8, 12, and 13 analogs that inspired the design of the library. Possible reactions include a nucleophilic addition to carbon 8 with Grignard reagents, treatment of berberine with elemental bromine yields 12-bromoberberine, which can serve as a handle for cross coupling reactions, and enamine condensations to carbon 13. (c) Workflow and methodology in our work

Here, we report an exhaustive in silico virtual screen of a representative library of 8-, 12-, and 13-alkyl and aryl berberine analogs (Figure 2b). The use of high throughput virtual screening (HVTS), which screens small molecule libraries against potential drug targets, has enabled rapid and efficient screening of large libraries of chemical entities (18,19,20). Molecular docking was used to determine the predicted binding affinity of each analog to each of the two DNA targets, time-dependent density functional theory (TD-DFT) calculations were invoked to predict the wavelength of maximal absorbance and relative energies of singlet and triplet excited states of each analog, and molecular dynamics (MD) was performed on berberine and selected analogs to simulate potential ligand-mediated stabilization of the G4DNA complex (Figure 2c). Since many DNA intercalators rely on pi-stack interactions or electrostatic attractions, we initially hypothesized that addition of aromatic systems to C8, C12, or C13 would provide an increase in binding affinity, and that loss of the cationic iminium at C8 would diminish binding affinity (21).

A library of 31 berberine analogs were screened against two biological targets, dsDNA and G4DNA, based on previously-reported crystal structures (PDB codes 3NP6 for dsDNA and 6JWD for G4DNA)(22,23). It was found that the impact of aryl and aliphatic substitution on DNA binding affinity is both position-dependent and target-dependent.
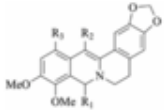
RESULTS

Molecular docking of the library of berberine analogs with dsDNA and G4DNA was completed using Autodock Vina. Docking parameters were determined from previously reported crystal structures, and a high degree of similarity in ligand positioning that was achieved between docked poses and the crystal structure demonstrates the predictivity of the docking parameters used. Results were quantified based on the free energy of binding (ΔG) in kcal/mol. The results are summarized in Figures 3.
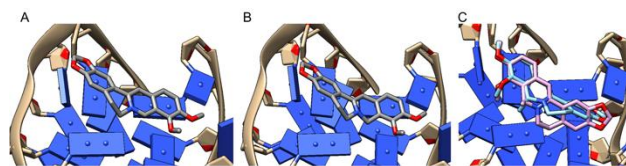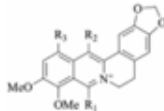

Figure 5. Binding poses of berberine and berberine analogs to G4DNA (a) Berberine 1 (ΔG = 2.6 kcal/mol) ((b) Dihydroberberine 2 (ΔG = 2.5 kcal/mol) (c) Both enantiomers of compound 8a. The structure in blue is the R enantiomer (ΔG = -0.1 kcal/mol), and the structure in purple is the S enantiomer (ΔG = 2.3 kcal/mol)
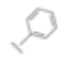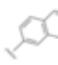
The lengthening of the alkyl chain on the carbon 8 analogs also resulted in decreased binding affinity of the compound to G4DNA. This could be attributed to steric clashes, in which members of the alkyl chain past the fourth carbon overlap with atoms of the receptor without being part of the binding interactions. This is thermodynamically unfavorable due to repulsive electron interactions between these clashing atoms, increasing the ΔG value. Differences were also observed between the R and S enantiomers of these analogs, with thermodynamic favorability of the R enantiomer for alkyl chains 4 carbons and shorter. This trend seems to be reversed for alkyl chains longer than 4 carbons, with the S enantiomer having lower ΔG values.
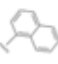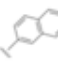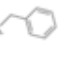
Compound 2, 8a-h

Compound	R₁	R₂	R₃	ΔG - dsDNA	ΔG - G4DNA
2	H	H	H	-6.2	2.5
8a	CH$_3$	H	H	R = -4.0, S = -4.1	R = -0.1, S = 2.3
8b	C$_2$H$_5$	H	H	R = -4.2, S = -3.8	R = 0.8, S = 1.4
8c	C$_4$H$_9$	H	H	R = -4.5, S = -4.3	R = 3.3, S = 5.0
8d	C$_6$H$_{13}$	H	H	R = -3.8, S = -3.6	R = 3.0, S = 2.5
8e	C$_8$H$_{17}$	H	H	R = -3.7, S = -3.6	R = 6.3, S = 1.5
8f	C$_{10}$H$_{21}$	H	H	R = -3.0, S = -3.2	R = 9.1, S = 3.4
8g	(phenyl)	H	H	R = -4.4, S = -3.4	R = 6.1, S = 9.8
8h	(naphthyl)	H	H	R = -2.1, S = -3.3	R = 9.3, S = 9.2
8i	(naphthyl)	H	H	R = -1.0, S = -2.2	R = 65.9, S = N/A

Compound 1, 12a-d, 13a-g

Compound	R₁	R₂	R₃	ΔG - dsDNA	ΔG - G4DNA
1	H	H	H	-5.6	2.6
12a	H	H	Br	-5.8	4.0
12b	H	H	(phenyl)	-5.9	25.7
12c	H	H	(naphthyl)	-6.0	35.5
12d	H	H	(naphthyl)	-6.8	N/A
13a	H	C$_4$H$_9$	H	-4.8	3.2
13b	H	C$_6$H$_{11}$	H	-4.8	7.4
13c	H	C$_8$H$_{17}$	H	-4.6	4.1
13d	H	C$_{10}$H$_{21}$	H	-4.3	8.2
13e	H	(branched chain)	H	-4.4	10.4
13f	H	(cyclohexyl)	H	-4.9	4.9
13g	H	(benzyl)	H	-4.2	11.1

Figure 3. Thermodynamics of the binding of the library berberine analogs to dsDNA (dsDNA) and G4DNA. Binding affinities are reported in kcal/mol, and represent the binding affinity of the most thermodynamically-stable predicted binding pose.

dsDNA Binding

Docking results for analogs with bromo-, phenyl-, and naphthyl- substitutions at the carbon 12 position were generally observed to have significantly greater binding affinities to dsDNA than analogs with substitutions at the carbon 8 and 13 positions, and some of these compounds exhibited greater binding affinity than berberine itself. Compounds with naphthyl groups on the carbon 12 had a binding affinity of -6.0 and -6.8 kcal/mol (Figure 4c), compound 12c and 12d, respectively.
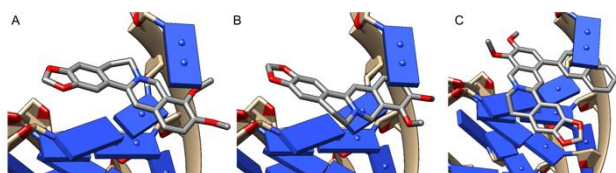
Figure 4. Most thermodynamically stable binding pose of representative compounds in our library to dsDNA (a) Berberine 1 (ΔG = -5.6 kcal/mol) (b) Dihydroberberine 2 (ΔG = -6.2 kcal/mol) (c) Compound 12d, the berberine analog with the best binding affinity to dsDNA (ΔG = -6.8 kcal/mol)

Interestingly, naphthyl additions to the carbon 8 position gave lower binding affinities than berberine, with ΔG values of -2.1 and -3.3 k/cal mol for the R and S enantiomers of compound 8h, respectively. The same trend can be seen in the R and S enantiomers of compound 8i, whose ΔG increased to -1.0 kcal/mol and -2.2 kcal/mol, respectively.

G4DNA Binding

Berberine analogs had significantly lower binding affinities to G4DNA than dsDNA. Unlike dsDNA, aliphatic chains on the carbon 8 positions demonstrated the best affinity in binding to G4DNA. The R enantiomer compound 8a had the lowest ΔG value of all analogs screened at -0.1 kcal/mol (Figure 5c). Additions of naphthyl groups at both carbon 8 and 12 greatly decreased the binding affinity of analogs 8h, 8i, 12c, and 12d to G4DNA. Compounds 8i and 12d were not able to dock to G4DNA. It is unclear why AutoDock Vina returned positive ΔG values for the DNA-berberine binding interaction.

Time Dependent Density Functional Theory

Time dependent density functional theory (TD-DFT) was utilized to study the excited state electronic structure of each compound. Moreover, the molecular orbital energies that resulted allowed us to probe whether berberine analogs undergo electronic transitions that can effectively produce singlet oxygen; the orbital energies that were obtained are summarized in Figure 6.

| Compound	E_{S0} (eV)	E_{S1} (eV)	E_{T1} (eV)	$\Delta E_{S0 \to S1}$ (H → L)	$\Delta E_{T1 \to S0}$ (H → L)	λ_{max} (nm)	Compound	E_{S0} (eV)	E_{S1} (eV)	E_{T1} (eV)	$\Delta E_{S0 \to S1}$ (H → L)	$\Delta E_{T1 \to S0}$ (H → L)	λ_{max} (nm)
1	-5.645	-2.701	-3.854	2.944	1.791	421	12a	-5.976	-2.851	-4.063	3.125	1.913	397
2	-4.735	-1.119	-2.447	3.616	2.288	343	12b	-5.837	-2.700	-3.953	3.137	1.884	396
8a	-4.775	-1.069	-2.400	3.706	2.375	335	12c	-5.822	-2.710	-3.942	3.112	1.880	399
8b	-4.768	-1.048	-2.382	3.720	2.396	334	12d	-5.718	-2.699	-3.962	3.019	1.756	411
8c	-4.688	-1.123	-2.447	3.565	2.241	348	13a	-5.720	-2.610	-3.892	3.110	1.828	399
8d	-4.685	-1.112	-2.430	3.573	2.255	347	13b	-5.719	-2.608	-3.892	3.111	1.827	399
8e	-4.861	-1.117	-2.436	3.744	2.425	331	13c	-5.725	-2.610	-3.880	3.115	1.845	398
8f	-4.620	-1.030	-2.343	3.590	2.277	346	13d	-5.814	-2.584	-3.876	3.230	1.938	384
8g	-4.766	-1.219	-2.506	3.547	2.260	350	13e	-5.724	-2.609	-3.893	3.115	1.831	398
8h	-4.771	-1.568	-2.563	3.203	2.208	387	13f	-5.814	-2.584	-3.876	3.230	1.938	384
8i	-4.699	-1.487	-2.419	3.212	2.280	386	13g	-5.761	-2.665	-3.940	3.096	1.821	401

Figure 6. Energy of the ground state, singlet excited state, and triplet excited state of berberine and its analogs from TD-DFT calculations. Electronic transitions are reported in eV, and the wavelength of maximal absorbance is reported in nanometers.
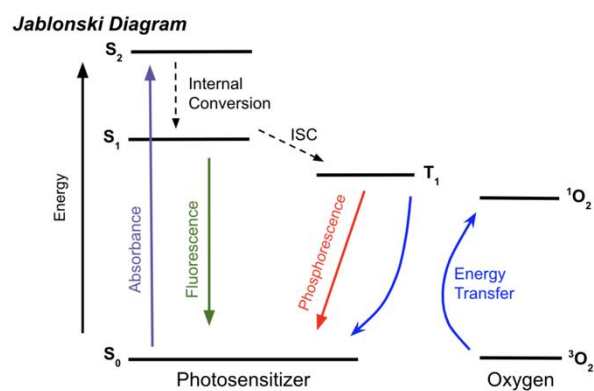
Figure 7. Jablonski Diagram depicting electronic transitions that occur as photosensitizers excite oxygen into singlet oxygen. Initial absorbance of a photon excites the ground state photosensitizer (S0) to the second excited state (S2), which undergoes rapid internal conversion to the first excited state (S1). This undergoes intersystem crossing to the first excited triplet state (T1), which can excite ground state triplet oxygen (3O2) to an excited singlet state (1O2).

Molecular dynamics was used to probe the interactions on timescale and potential stabilizing effects of the binary complex between G4DNA and berberine, dihydroberberine, and 8-methylberberine. Specifically, stabilization over time of the G4DNA by berberine and the two analogs was calculated in GROMACS and displayed in Figure 8a, and the average RMSD was calculated over the same time interval, displayed in Figure 8b. G4DNA with berberine was observed to have a lower maximum RMSD value than G4DNA with dihydroberberine and 8-methylberberine. Unpaired t-testing revealed that the differences in RMSD between berberine, dihydroberberine, and G4DNA are insignificant at a 95% confidence interval. However, the difference between RMSD G4DNA and 8-methylberberine is statistically significant, suggesting a destabilization of G4DNA by 8-methylberberine.
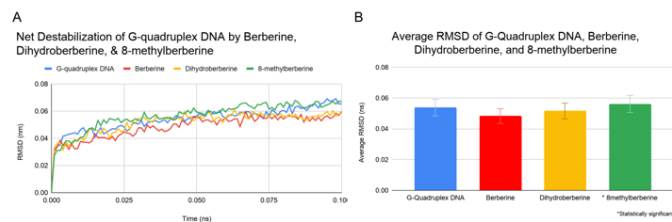
Figure 8. Root-mean-square deviation of atomic position (RMSD) calculations from molecular mechanisms (a) Average RMSD of G4DNA, G4DNA with berberine, G4DNA with dihydroberberine, and G4DNA with 8-methylberberine over 0.1 nanosecond in water (b) Net Destabilization of G4DNA by berberine, dihydroberberine, and 8-methylberberine

DISCUSSION

Molecular docking, TD-DFT excited state calculations, and molecular dynamics simulations were performed to investigate the structure relationship activity (SAR) on the impact of aliphatic and aromatic side chains at C8, 12, and 13 in binding affinities towards double stranded DNA (dsDNA) and G4DNA. While the G4DNA's binding affinity appears positive, the results were deemed predictive because the most thermodynamically favorable binding pose was accurately predicted. Analogs with the highest binding affinity to dsDNA were the 12-substituted analogs, which had binding affinities of -5.8 to -6.8 kcal/mol compared to a binding affinity of -5.6 kcal/mol for berberine 1. The aromatic 12-substituted analogs performed the best overall with binding affinities comparable to berberine 1, likely due to the increased number of pi stacking interactions.

Contrary to our initial hypothesis, berberine analogs with aromatic substitution did not always have the highest binding affinity to either dsDNA or G4DNA targets. Rather, the effect of aryl versus aliphatic substitution on DNA binding appears to be dependent on not only the nature of the substituted group, but also the carbon position (C8, C12, C13) substituted and on the nucleic acid target - as different trends were observed in binding affinity to dsDNA and G4DNA. Moreover, it appears that a loss of the persistent cation in the isoquinolinium core of berberine, as in the case of dihydroberberine and any 8-alkyl or 8-aryl analog, is not necessarily detrimental to DNA binding. Moreover, against initial expectations, molecular dynamics simulations do not seem to indicate net stabilization of the G-quadruplex-ligand binary complex.

Visual inspection of the docked poses suggest that steric effects are operative in the superior binding affinity of 8-alkyl berberine analogs in G4DNA (Figure 3, compounds 8a, 8b, 8c, and 8d). The crystal structure positions the compound in a manner where C8 directly faces the DNA, forcing a substituent on carbon 8 to penetrate further in and have more interactions with the G4DNA. However, the relatively poor binding affinity of a larger substituent such as the aromatic compound 8g is potentially driven by greater steric encumbrance to intercalate in G4DNA. Aliphatic 8-substituted analogs in G4DNA's R enantiomers are more thermodynamically favorable than S enantiomers for 4 carbons and shorter, which can be explained by a reduced amount of steric hindrance in the direction of the S enantiomers. The shorter chains probably allow for the molecule to interculate more closely into G4DNA, however longer chains are too sterically hindered to allow the analogs to bind in more thermodynamically favorable positions.

The analogs with the lowest binding affinity to G4DNA were the aromatic substituents, whereas the analogs with the best binding affinity to dsDNA were the aromatic substituents. The affinity for aliphatic chains in G4DNA can be attributed to G4DNA's complex folding, exacerbating the problems of steric hindrance (26). The higher variation of binding affinities against G4DNA indicated that the smaller binding pockets result in greater variation in the ΔG binding affinities as bigger molecules like compound 12b are too sterically hindered to bind in more thermodynamically favorable conformer poses.

Compound 8a was observed to have the highest binding affinity to G4DNA, however molecular dynamics simulations revealed that this compound destabilizes G4DNA, with an average RMSD value of 0.0562 ns, while G4DNA has an average RMSD value of 0.0538 ns. Comparatively, berberine and dihydroberberine had much higher stabilization capabilities, with average RMSD values of 0.0483 and 0.0516 ns, respectively, lower than the average G4DNA RMSD value.

Through TDDFT calculations, we were able to determine that the berberine analogs undergo an electronic transition that is sufficient for the production of singlet oxygen. Further studies on the lifetime of the triplet state of the berberine analogs is necessary to accurately understand the photosensitizing ability of berberine. One limitation with the use of berberine analogs is the blueshift observed in the maximum wavelength of absorbance. Many biomolecular entities, such as DNA and aromatic amino acids, have absorbance in the ultraviolet range, and photodynamic therapy with berberine analogs could possibly result in undesired side effects (27).

Through molecular docking, time-dependent density functional theory (TD-DFT), and molecular dynamics (MD) simulations we present an exhaustive structure-activity relationship (SAR) between berberine and its C8, C12, and C13 analogs with respect to their binding affinity to both double stranded DNA (dsDNA) and G-quadruplex DNA (G4DNA). While this study primarily focused on computational work and rapid in silico screening of such compounds, it provides the basis for future work in the chemical synthesis and in vitro evaluation of hit structures and their DNA-binding efficacy.

MATERIALS AND METHODS

Molecular Mechanics Pre-Optimization Avogadro, a cross-platform molecular editor, was used to create three-dimensional computational models of berberine and each of the studied analogs (28). Prior to density functional theory (DFT) geometry optimization, each model was initially optimized by molecular mechanics using the Merck Molecular Forcefield (MMFF94) to 10,000 steps. Input files for DFT structural optimizations were created on Avogadro.

DFT Structural Optimization Density functional theory (DFT) was used to calculate quantum mechanically minimized molecular geometries. ORCA, an ab initio quantum mechanical molecular modeling software, was used in tandem with Avogadro's functionality to generate ORCA input files to compute the DFT optimized structure of berberine and each analog (29). An implicit conductor-like polarizable continuum (CPCM) solvation model of water was used to simulate the conditions of an

aqueous environment. B3LYP, a hybrid functional, was chosen for the calculation due to its low computational cost compared to other traditional functionals, as well as its acceptance in the scientific community for creating low parameter, accurate results (30,31). All DFT calculations were carried out to normal convergence thresholds. Additionally, time-dependent density functional theory (TD-DFT) was used to model the excited singlet and triplet states of berberine and its analogs. The RIJCOSX approximation method was used to greatly accelerate the calculation with negligible decrease in accuracy and significant reduction of computational expense.

AutoDockTools AutoDockTools (ADT), a part of the MGLTools suite, is a graphical user interface that allows for the preparation and generation of coordinate files for use in AutoDock Vina (32,33). To prepare the dsDNA and G4DNA for the docking procedure, ADT was used to identify the receptors as a macromolecule, which adds Gasteiger charges to the molecule and merges non-polar hydrogens. The search space for the ligand was also chosen at this stage, modelled after 3NP6 for dsDNA and 6JWD for G4DNA. Each ligand was prepared by importing the coordinate file into ADT as a ligand, upon which the Gasteiger charges would be computed and applied to the molecule. The identification of the torsion tree root allowed the number of rotatable bonds to be set, allowing for maximum conformity of the ligand to induce fit into the specified search grid.

AutoDock Vina AutoDock Vina (ADV) is an open source molecular docking program (34). Configuration of Vina included the definition of the search grid from ADT. Additionally, Vina was queried to generate 15 conformers of each ligand rather than the default 9 binding modes in order to avoid omission of possible conformers. The exhaustiveness value of the search was doubled from the default 8 to 16 in order to generate models from more computationally exhaustive methods. The validity of the docking parameters used was first assessed by comparing the predicted highest-affinity binding pose of berberine to dsDNA with that which was previously reported in its crystal structure (PDB 3NP6), and these were found to be consistent.

UCSF Chimera/ChimeraX Visual analysis to determine the accuracy of the berberine molecule's computationally determined binding mode to that of the crystal structure shown in 3NP6 and 6JWD was done in UCSF Chimera and UCSF ChimeraX, a molecular visualization program (35,36).

GROMACS GROMACS, or the GROningen MAchine for Chemical Simulations, is a molecular dynamics (MD) package that simulates interactions between proteins and ligands (37). GROMACS was used to carry out high-level molecular dynamics simulations in regards to the interactions between the most thermodynamically favourable conformers of berberine, dihydroberberine, and G4DNA using the AMBER99SB forcefield and an explicit TIP3 water solvation model. Energy minimization (EM) was conducted in order to minimize the structure and remove clashes within the system. An equilibration step was conducted to meet temperature and pressure constraints imposed by the MD simulation. Configuration of the forcefield using AMBER99SB parametrics and bond-charge correction (BCC) charges on the ligand level was carried out on the ACPYPE Web Server (38). Additional time-dependent RMSD calculations to determine net stabilization of the DNA were also carried out using GROMACS. MDWeb was used to generate the structure of each system MD was simulated for in the PDB format with GROMACS trajectories for visualization in Chimera (39).

DFT, TD-DFT, molecular docking, and molecular dynamics calculations were performed on a Dell PowerEdge 710 server with a 24 core Intel Xeon X5660 processor @ 2.80GHz and 32GB RAM.

Wavelength of Excitation

$\lambda = hc/E = ((6.626*10^{-34}Js)(3.00*10^8 m/s)*10^9 nm/m)/((LUMO-HOMO)*1.602*10^{-19}J/eV)$

The minimum energy in electron-volts (eV) to excite Berberine and its analogs was found by subtracting the lowest unoccupied molecular orbital (LUMO) by the highest occupied molecular orbital (HOMO). Avogadro was used to view the HOMO and LUMO orbital energies calculated through time-dependent density functional theory (TD-DFT) calculations in ORCA.

ASDRP for his guidance with initial setup and remote access to the server.

AUTHOR INFORMATION

REFERENCES

(1) Grycová, Lenka, et al. "Quaternary Protoberberine Alkaloids." Phytochemistry, vol. 68, no. 2, 2007, pp. 150–175., doi:10.1016/j.phytochem.2006.10.004.

(2) Wang, Ye, et al. "The Anti-Cancer Mechanisms of Berberine: A Review." Cancer Management and Research, Volume 12, 2020, pp. 695–702., doi:10.2147/cmar.s242329.

(3) Stermitz, F. R., et al. "Synergy in a Medicinal Plant: Antimicrobial Action of Berberine Potentiated by 5-Methoxyhydnocarpin, a Multidrug Pump Inhibitor." Proceedings of the National Academy of Sciences, vol. 97, no. 4, Apr. 2000, pp. 1433–1437., doi:10.1073/pnas.030540597.

(4) Wang, Haoran, et al. "Metformin and Berberine, Two Versatile Drugs in Treatment of Common Metabolic Diseases." Oncotarget, vol. 9, no. 11, Nov. 2017, doi:10.18632/oncotarget.20807.

(5) Lau, Chi-Wai, et al. "Cardiovascular Actions of Berberine." Cardiovascular Drug Reviews, vol. 19, no. 3, July 2006, pp. 234–244., doi:10.1111/j.1527-3466.2001.tb00068.x.

(6) Tillhon, Micol, et al. "Berberine: New Perspectives for Old Remedies." Biochemical Pharmacology, vol. 84, no. 10, 2012, pp. 1260–1267., doi:10.1016/j.bcp.2012.07.018.

(7) Shebs, Stan. "Berberis Trifoliolata Fruit." Wikimedia Commons, 2005, commons.wikimedia.org/w/index.php?curid=173295.

(8) Krey, A. K., and F. E. Hahn. "Berberine: Complex with DNA." Science, vol. 166, no. 3906, July 1969, pp. 755–757., doi:10.1126/science.166.3906.755.

(9) Hirakawa, Kazutaka, et al. "The Mechanism of Guanine Specific Photooxidation in the Presence of Berberine and Palmatine: Activation of Photosensitized Singlet Oxygen Generation through DNA-Binding Interaction." Chemical Research in Toxicology, vol. 18, no. 10, 2005, pp. 1545–1552., doi:10.1021/tx0501740.

(10) Callaghan, Susan, and Mathias O. Senge. "The Good, the Bad, and the Ugly – Controlling Singlet Oxygen through Design of Photosensitizers and Delivery Systems for Photodynamic Therapy." Photochemical & Photobiological Sciences, vol. 17, no. 11, 2018, pp. 1490–1514., doi:10.1039/c8pp00008e.

(11) Ragás, Xavier, et al. "Singlet Oxygen in Antimicrobial Photodynamic Therapy: Photosensitizer-Dependent Production and Decay in E. Coli." Molecules, vol. 18, no. 3, 28 Feb. 2013, pp. 2712–2725., doi:https://doi.org/10.3390/molecules18032712.

(12) Moraca, Federica, et al. "Ligand Binding to Telomeric G-Quadruplex DNA Investigated by Funnel-Metadynamics Simulations." Proceedings of the National Academy of Sciences, vol. 114, no. 11, 2017, doi:10.1073/pnas.1612627114.

(13) Iwasa, Kinuko, et al. "Antimicrobial Activity of 8-Alkyl- and 8-Phenyl-Substituted Berberines and Their 12-Bromo Derivatives." Journal of Natural Products, vol. 61, no. 9, 1998, pp. 1150–1153., doi:10.1021/np980044+.

(14) Wang, Bo, et al. "Syntheses and Structure–Activity Relationships in Growth Inhibition Activity against Human Cancer Cell Lines of 12 Substituted Berberine Derivatives." Molecules, vol. 25, no. 8, 2020, p. 1871., doi:10.3390/molecules25081871.

(15) Lee, Dong-Ung, et al. "Effects of 13-Alkyl-Substituted Berberine Alkaloids on the Expression of COX-II, TNF-α, INOS, and IL-12 Production in LPS-Stimulated Macrophages." Life Sciences, vol. 73, no. 11, 2003, pp. 1401–1412., doi:10.1016/s0024-3205(03)00435-1.

(16) Zhang, Lei, et al. "Synthesis and Cytotoxicity Evaluation of 13-n-Alkyl Berberine and Palmatine Analogues as Anticancer Agents." Molecules, vol. 17, no. 10, 2012, pp. 11294–11302., doi:10.3390/molecules171011294.

(17) Rodrigues, Catarina A. B., et al. "Synthesizing a Berberine Derivative and Evaluating Antimicrobial Activity To Reinforce with Students the Potential Significance of Small Chemical Structure Changes for Biological Systems." Journal of Chemical Education, vol. 95, no. 3, 2018, pp. 492–495., doi:10.1021/acs.jchemed.7b00458.

(18) Dhasmana, Anupam, et al. "High-Throughput Virtual Screening (HTVS) of Natural Compounds and Exploration of Their Biomolecular Mechanisms." New Look to Phytomedicine, 2019, pp. 523–548., doi:10.1016/b978-0-12-814619-4.00020-3. - Suhitha, Sivasubramanian, et al. "Structure Based Design of Compounds from Natural Sources for Diabetes and Inflammation." Bioinformation, vol. 8, no. 23, 2012, pp. 1125–1131., doi:10.6026/97320630081125.

(19) Kumari, Madhulata, et al. "High Throughput Virtual Screening to Identify Novel Natural Product Inhibitors for MethionyltRNA-Synthetase of Brucella Melitensis." Bioinformation, vol. 13, no. 1, 2017, pp. 8–16., doi:10.6026/97320630013008.

(20) Kontoyianni, Maria. "Docking and Virtual Screening in Drug Discovery." Methods in Molecular Biology Proteomics for Drug Discovery, 2017, pp. 255–266., doi:10.1007/978-1-4939-7201-2_18.

(21) Mignon, P. "Influence of the - Interaction on the Hydrogen Bonding Capacity of Stacked DNA/RNA Bases." Nucleic Acids Research, vol. 33, no. 6, 2005, pp. 1779–1789., doi:10.1093/nar/gki317.

(22) Ferraroni, Marta, et al. "X-Ray Diffraction Analyses of the Natural Isoquinoline Alkaloids Berberine and Sanguinarine Complexed with Double Helix DNA d(CGTACG)." Chemical Communications, vol. 47, no. 17, 2011, p. 4917., doi:10.1039/c1cc10971e.

(23) Wang, Fei, et al. "Colchicine Selective Interaction with Oncogene RET G-Quadruplex Revealed by NMR." Chemical Communications, vol. 56, no. 14, 2020, pp. 2099–2102., doi:10.1039/doccc00221f.

(24) Derosa, M. "Photosensitized Singlet Oxygen and Its Applications." Coordination Chemistry Reviews, vol. 233-234, 2002, pp. 351–371., doi:10.1016/s0010-8545(02)00034-6.

(25) Alberto, Marta Erminia, et al. "Rational Design of Modified Oxobacteriochlorins as Potential Photodynamic Therapy Photosensitizers." International Journal of Molecular Sciences, vol. 20, no. 8, 2019, p. 2002., doi:10.3390/ijms20082002.

(26) Ida, Jeunice, et al. "G-Quadruplexes as An Alternative Recognition Element in Disease-Related Target Sensing." Molecules, vol. 24, no. 6, 2019, p. 1079., doi:10.3390/molecules24061079.

(27) Schmid, Franz-Xaver. "Biological Macromolecules: UV-Visible Spectrophotometry." Encyclopedia of Life Sciences, 2001, doi:10.1038/npg.els.0003142.

(28) Marcus D Hanwell, Donald E Curtis, David C Lonie, Tim Vandermeersch, Eva Zurek and Geoffrey R Hutchison; "Avogadro: An advanced semantic chemical editor, visualization, and analysis platform" Journal of Cheminformatics 2012, 4:17.

(29) Neese, Frank. "The ORCA Program System." WIREs Computational Molecular Science, vol. 2, no. 1, 2011, pp. 73–78., doi:10.1002/wcms.81.

(30) Lee, Chengteh, et al. "Development of the Colle-Salvetti Correlation-Energy Formula into a Functional of the Electron Density." Physical Review B, vol. 37, no. 2, 1988, pp. 785–789., doi:10.1103/physrevb.37.785.

(31) Becke, Axel D. "Density-Functional Thermochemistry. III. The Role of Exact Exchange." The Journal of Chemical Physics, vol. 98, no. 7, 1993, pp. 5648–5652., doi:10.1063/1.464913.

(32) Michel F. Sanner. Python: A Programming Language for Software Integration and Development. J. Mol. Graphics Mod., 1999, Vol 17, February. Pp57-61

(33) Morris, G. M., Huey, R., Lindstrom, W., Sanner, M. F., Belew, R. K., Goodsell, D. S. and Olson, A. J. (2009) Autodock4 and AutoDockTools4: automated docking with selective receptor flexiblity. J. Computational Chemistry 2009, 16: 2785-91.

(34) O. Trott, A. J. Olson, AutoDock Vina: improving the speed and accuracy of docking with a new scoring function, efficient optimization and multithreading, Journal of Computational Chemistry 31 (2010) 455-461

(35) Pettersen, E.F., Goddard, T.D., Huang, C.C., Couch, G.S., Greenblatt, D.M., Meng, E.C., and Ferrin, T.E. "UCSF Chimera - A Visualization System for Exploratory Research and Analysis." J. Comput. Chem. 25(13):1605-1612 (2004).

(36) UCSF ChimeraX: Meeting modern challenges in visualization and analysis. Goddard TD, Huang CC, Meng EC, Pettersen EF, Couch GS, Morris JH, Ferrin TE. Protein Sci. 2018 Jan;27(1):14-25.

(37) M.J. Abraham, D. van der Spoel, E. Lindahl, B. Hess, and the GROMACS development team, GROMACS User Manual version 2019, http://www.gromacs.org

(38) Sousa da Silva, A.W., Vranken, W.F. ACPYPE - AnteChamber PYthon Parser interfacE. BMC Res Notes 5, 367 (2012). https://doi.org/10.1186/1756-0500-5-367

(39) Adam Hospital, Pau Andrio, Carles Fenollosa, Damjan Cicin-Sain, Modesto Orozco, Josep Lluís Gelpí MDWeb and MDMoby: an integrated web-based platform for molecular dynamics simulations. Bioinformatics, 2012, 28(9):1278-1279.